Energy consumption mechanism simulation and experimental study of reciprocating vibration for Chinese wolfberry picking

Song Mei[1,2], Dunbing Tang[1*], Zhigang Shi[3], Zhiyu Song[2], Cheng Shen[2*]

(1. *College of Mechanical and Electrical Engineering, Nanjing University of Aeronautics and Astronautics, Nanjing 210016, China*;
2. *Nanjing Institute of Agricultural Mechanization, Ministry of Agriculture and Rural Affairs, Nanjing 210014, China*;
3. *Institute of Chinese Wolfberry Science, Ningxia Academy of Agriculture and Forestry Sciences, Yinchuan 750002, China*)

Abstract: In order to find out the matching principle of excitation force and energy consumption of reciprocating vibrating Chinese wolfberry picking device, the energy consumption mechanism of reciprocating vibrating Chinese wolfberry picking device is studied. According to the structural characteristics and operating principle of the picking device, the no-load and load movement and force characteristics of the crank bearing and vibrating component are analyzed, and the theoretical model of energy consumption of the reciprocating vibration picking device is jointly constructed, and the simulation analysis is carried out. The results show that the vibrating component and load mass have a significant influence on torque, the load air resistance phase has a significant effect on torque, and the load air resistance and friction coefficient have no significant influence on torque. Subsequently, by building an AC servo motor torque detection system and a torque sensing detection system, verification experiments are carried out, the maximum torque of the preset system is 1.3 N·m, the rated power is 400 W, the motor frequency is 20 Hz, the amplitude is 15 mm, and the total mass of the vibrating component is 0.143 kg. Test results show that, the no-load operation, the change trend of detected torque is consistent with simulation, the torque model is verified to be accurate. The maximum torque of simulation and detection are 0.52 N·m and 0.57 N·m respectively, and the error between test and simulation is 9.6%. For load operation, the maximum torque of five groups of branch loads of 20 g, 60 g, 100 g, 140 g, 180 g and 220 g are detected to be 0.73 N·m, 0.74 N·m, 0.75 N·m, 0.82 N·m and 0.83 N·m, respectively, and the relationship model between load and torque is obtained by fitting. The research results can provide a theoretical basis which can configure a suitable motor in the reciprocating vibration Chinese wolfberry picking device with a certain load limit.

Keywords: Chinese wolfberry branches, vibration component, load, torque, power

DOI: 10.25165/j.ijabe.20241704.8939

Citation: Mei S, Tang D B, Shi Z G, Song Z Y, Shen C. Energy consumption mechanism simulation and experimental study of reciprocating vibration for Chinese wolfberry picking. Int J Agric & Biol Eng, 2024; 17(4): 146–155.

1 Introduction

Chinese wolfberry originated in China and are mostly distributed in temperate and subtropical regions, such as Ningxia, Inner Mongolia, Gansu and Xinjiang, with a total area of nearly 200 000 hm^2[1,2] .Chinese wolfberry is one of the most important characteristic cash crops in China, which is rich in nutrition and high medicinal value[3]. The production and management costs of Chinese wolfberry have increased year by year, but the average selling price of Chinese wolfberry has not increased much in the past 20 years and the whole process of mechanized management has reduced the production cost, which is the way out for the sustainable and healthy development of the Chinese wolfberry industry. At present, mechanized harvesting of Chinese wolfberry is a weak link, and the cost of manual picking accounts for 40% of the total cost, so it is imperative to replace manual labor with machinery[4].

In recent ten years, researchers from domestic research institutes and universities have made various attempts for the improvement of mechanization of wolfberry harvesting, and learned from foreign berry harvesting methods such as blueberry and raspberry, including vibrating type, comb brush type, shear type, pneumatic type, etc[5]. Through several years of exploration of the biological characteristics of Chinese wolfberry and the improvement of picking devices, vibration picking has been considered to be the best method for the wolfberry picking[6]. Based on this, the domestic research is mainly carried out from the small portable and large-scale self-propelled Chinese wolfberry picking. Combining the small portable Chinese wolfberry harvesting device with manual operation, it is expected that the work efficiency will be improved by more than three times and the labor intensity can be reduced[7,8], Zhang et al.[9] designed a shaking Chinese wolfberry harvester, and the experiment showed that the net recovery rate was 93.52%, and the damage rate was 2.54%, which met the quality requirements of Chinese wolfberry harvesting and was 5.5 times that of manual labor; Cao et al.[10] designed a hand-held Chinese wolfberry picker, the basic principle of which is to use an eccentric mechanism to vibrate the branches, so that the direction of Chinese wolfberry fruit changes several times in an instant, until the inertial force reaches the requirement of fruit removal, and the fruit removal effect is good. Inspired by the tactile sensation of human and hand

Received date: 2023-12-03 **Accepted date:** 2024-07-09

Biographies: Song Mei, Associate Researcher, research interest: agricultural mechanization engineering for fruits, Email: meisong@caas.cn; **Zhigang Shi**, Researcher, research interest: agricultural engineering, Email: 237518963@qq.com; **Zhiyu Song**, Researcher, research interest: agricultural mechanization engineering, Email: songzhiyu@caas.cn.

***Corresponding author: Dunbing Tang**, Professor, research interest: intelligent agriculture, College of Mechanical and Electrical Engineering, Nanjing University of Aeronautics and Astronautics, No.29 Yudao Street, Qinhuai District, Nanjing 210016, China. Tel: +86-13776639985, Email: d.tang@nuaa.edu.cn; **Cheng Shen**, Associate Professor, research interest: agricultural engineering, Nanjing Institute of Agricultural Mechanization, Ministry of Agriculture and Rural Affairs, No.100 Liuying, Xuanwu District, Nanjing 210014, China. Email: shencheng@caas.cn.

nerves, Zhao et al.[11] proposed an untethered intelligent soft gripper to adaptively and effectively pick fruits. Qin et al.[12] invented a vibrating Chinese wolfberry picking machine, the principle of reciprocating swing is used by which to drive the four-claw rod teeth to knock the branches until the fruit falls off, and the operation effect is better than original machines. The small portable Chinese wolfberry vibrating picking device mentioned above has the advantages of simple structure, small size, light weight, portability, etc. but its working efficiency is low, and the degree of manual dependence is high. It was required to manually hold the handle of the machine to catch and fix the fruit-bearing branches and pick them by vibration, and the picking efficiency is 3-5 times that of pure labor. However, the current sharp shortage of labor, rising labor costs, large scale of Chinese wolfberry planting and strict timeliness requirements[13], are not critical issues of Chinese wolfberry industry. we must learn from the above harvesting methods, and study the continuous harvesting device suitable for large-scale self-propelled Chinese wolfberry to solve the fundamental problem.

The research on large-scale self-propelled Chinese wolfberry picking technology is as follows: He et al.[14] analyzed the structural characteristics and research status of the vibrating harvesting device that is currently widely used, and proposed a new vibrating harvesting mode based on gear-five-link mechanism, which has stable force transmission and can realize a variety of complex movement trajectories to improve the picking rate of ripe Chinese wolfberry fruits and reduce the damage to unripe fruits and flowers. Zhang et al.[15] established a mechanical model of forced vibration picking according to the mechanism of Chinese wolfberry vibrating picking, and then optimized and simulated the working parameters of the vibrating Chinese wolfberry harvester with MATLAB tools, and finally the experimental device, experimental platform and prototype of self-propelled Chinese wolfberry harvester including various harvesting principles were trial-produced. Liu et al.[16] from the Agricultural Machinery Technology Extension Center of Jinghe County, Xinjiang Uygur Autonomous Region, introduced a large-scale vibrating Chinese wolfberry harvester, which adopts the principle of low-frequency and high-amplitude vibration, with a supporting power of 30 horsepower and a shaking vibration of about 90 pieces/m^2. The net harvesting rate of summer fruit is about 90%, which is serious by mistake and less harmful to Chinese wolfberry, but the shaking Chinese wolfberry harvester cannot realize continuous harvesting, which limits the improvement of its efficiency to a certain extent. Peng et al.[17] designed a precision clamping vibration Chinese wolfberry picking device, which clamped the branches by double-sided telescopic and adjusted the fork gap and adopted a low-frequency and high-amplitude vibration mode to achieve efficient picking of Chinese wolfberry, and the operation effect was good, but the efficiency was low.

Based on the above analysis, it is evident that the current research directions in this field are quite fragmented. For instance, the predominant approach for vibration currently relies on oscillating teeth with large gaps, low frequencies, and low amplitudes. However, there are significant challenges for these vibration components including high energy consumption[18-21], limited frequency scalability, slow movement, inability to achieve continuous harvesting, increased risk of erroneous selection and missed targets, and a higher likelihood of fruit damage from impacts. The authors opted for a reciprocating high-frequency and low-amplitude vibration mode to design a portable device for Chinese wolfberry picking. These modified components were integrated on both sides of a large-scale Chinese wolfberry picking machine, aiming to enhance the Chinese wolfberry cultivation mode and facilitate the integration of agricultural machinery and agronomy[22]. However, during the prototype testing phase, it was observed that the picking components were prone to failures in variable load operating conditions. To address these issues, it becomes essential to investigate the energy consumption mechanism of the core unit of the picking components, i.e., the drive motor. Therefore, this study focuses on examining the energy consumption mechanism of reciprocating vibration-based Chinese wolfberry picking. Through the construction of energy consumption model, simulation analysis and experimental verification, the study aims to identify the parameters that influence energy consumption and design guidelines for operating power optimization.

2 Structure and working principle of vibrating device

2.1 Structure of vibrating component

The reciprocating vibration Chinese wolfberry fruit removal machine consists primarily of a power supply and frequency conversion control box, a DC motor, a crank, bearings, a guide plate, a slider, an end cover, and gear shaping. The schematic diagram of the structure is shown in Figure 1.

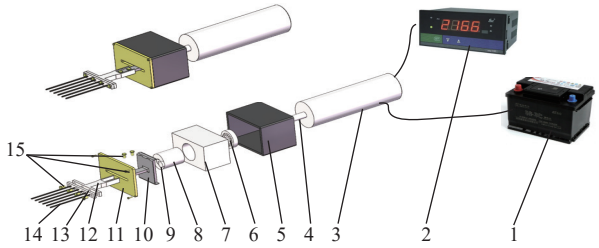

1. Power . 2.Frequency conversion controller. 3. Motor. 4. Motor output shaft. 5. Outer frame of coupling. 6. Axial bearing. 7. Inner frame of coupling . 8. Disc hinged with power shaft. 9. Crank tip bearing. 10. Forced to move the slider. 11. End cover. 12. Fork connector 1. 13. Fork connector 2. 14. U-shaped fork bar. 15. Hinges

Figure 1 Schematic diagram of reciprocating vibration structure

As shown in Figure 1, it can be observed that the reciprocating vibration Chinese wolfberry fruit removal machine is driven by a DC motor. The crank end bearing interact with the guide plate, and the guide plate is connected to the slider, which is constrained to move within a specific range by the end cover and it forces the slider, along with the gear shaping fixed at the other end, to achieve high-speed reciprocating motion. The branches are placed between the gear shaping steel bars, and the reciprocating motion of which is facilitated by the adjacent steel bars. The highlight of this mechanism is the use of a disc hinged to the power shaft instead of the traditional crank. The disc is equipped with bearings to enhance the system's smooth operation. This design is suitable for light-load, high-frequency, and low-amplitude reciprocating motion. Compared to the traditional crank-slider mechanism, not only the space for installing the vibrating components is saved, but also the weight and energy consumption is reduced.

2.2 principle of operation

During the fruit removal process, the operator holds the handle of the motor shell and places mature Chinese wolfberry branches between the teeth of the device, and the fruiting device is then activated, causing the branches to undergo reciprocating movement with a certain frequency and amplitude under the influence of

adjacent tooth shaping. As the branches move back and forth, Chinese wolfberries are influenced by inertial forces. When the inertia force exceeds the binding force between the Chinese wolfberry and the fruit stalk, or between the fruit stalk and the fruit pedicle, the wolfberries detach from the branches and enter the collection device. The teeth shaping mechanism acts on different sections of the branch, allowing for the picking of mature wolfberries within a specific area above and below the striking point. Finally, the collected Chinese wolfberries are subjected to centralized processing and analysis to assess their condition.

3 Construction and simulation analysis of energy consumption model for vibrating components

3.1 Construction of energy consumption model for vibrating components

3.1.1 Analysis of reciprocating vibration motion

To further simplify Figure 1, as shown in Figure 2a, the motion of the mechanism is that the crank end center moves circumferentially around the center, with the outer end of the bearing moving up and down within the guide plate. The slider, fixed to the guide plate, is constrained to move left and right along the end groove on the end cover. The gear shaper, fixed in the middle of the slider, reciprocates within the designated interval in the middle opening of the end cover. The relationship between the gap between adjacent steel bars of the gear and the critical exchange of forced vibration branches needs to be calculated theoretically. Considering the picking mechanism of wolfberries with reciprocating forced vibration, it is important to note that weather the angle between the vibrating component and the plumb line during operation is favorable for the quick separation of the fruit. This angle needs to be taken into account when modeling, as follows.

From Figure 2a, it can be observed that the crank rotates in the x-y plane, while the reciprocating vibration components (including sliders, connecting mechanisms, and fork rods) move back and forth along the x'-axis. The angle between the vibrating components and the horizontal x-axis is φ. By rotating the entire component by φ, the projection of the crank end corresponds to the x and y axes, and the motion characteristics along the x' and y' axes can be summarized as follows:

$$\begin{cases} s_x = r\cdot\cos\theta\cdot\cos\varphi = r\cdot\cos\omega t\cdot\cos\varphi \\ a_x = \dfrac{d}{dt}\left(\dfrac{ds_x}{dt}\right) = -r\cdot\omega^2\cos\omega t\cdot\cos\varphi \\ v_{x'} = -r\omega\sin\omega t \\ a_{x'} = -r\cdot\omega^2\cos\omega t \\ s_y = r\cdot\sin\theta\cdot\cos\varphi = r\cdot\sin\omega t\cdot\cos\varphi \\ a_y = \dfrac{d}{dt}\left(\dfrac{ds_y}{dt}\right) = -r\cdot\omega^2\sin\omega t\cdot\cos\varphi \\ a_{y'} = -r\cdot\omega^2\sin\omega t \\ \omega = \dfrac{2\pi}{T} = 2\pi\cdot N \end{cases} \quad (1)$$

where, s_x is displacement of the crank end bearing and the center of the vibrating component along x-axis, m; a_x is acceleration of the crank end bearing and the vibrating component along x-axis, m/s^2; $v_{x'}$ is reciprocating speed of the vibrating component along the x' axis, m/s; $a_{x'}$ is acceleration of the crank end bearing and vibrating component along the x' axis, m/s^2; s_y is displacement of the crank end bearing along y-axis, m; a_y is acceleration of the crank end bearing along y-axis, m/s^2; $a_{y'}$ is acceleration of the crank end bearing along y'-axis, m/s^2; r is crank length, m; ω is angular velocity of the crank around the origin, rad/s; φ is angle between the vibrating component and horizontal x-axis, rad; T is time taken by the crank to complete one rotation around the origin, s; N is motor speed, r/s; t is rotation time, s.

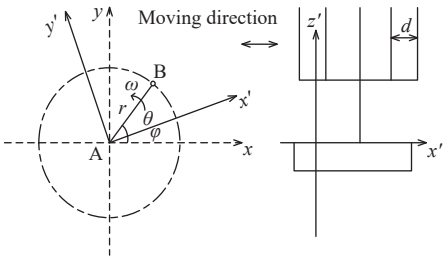

a. Kinematic diagram for reciprocating vibration device

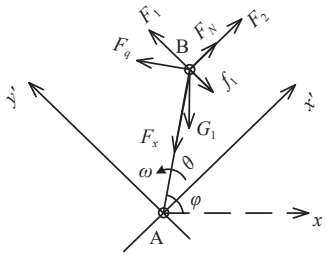

b. Stress diagram of crank tip bearing

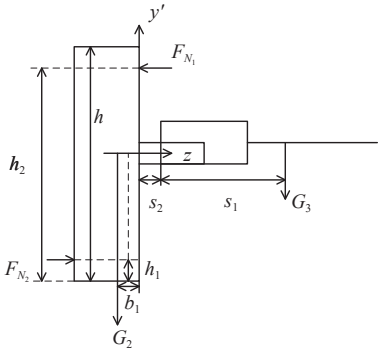

c. Force analysis diagram of slider

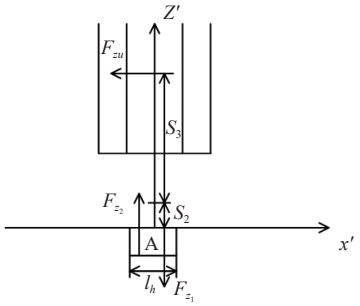

d. Force analysis of vibration device with load

Figure 2 Exploded diagram for reciprocating vibration device

3.1.2 Force analysis of the crank terminal

The contact between the crank terminal rolling bearing and the slider, with rolling friction between them is involved in the motion characteristics of this mechanism. In the direction where there is no displacement change for the moving components and the rear side fork rod, the crank does not impart inertia force to the contact moving component. It only imparts inertia force to the bearing hinged at the end of the crank. Additionally, under the influence of the traction force, only the bearing maintains a constant speed motion in the circumferential direction and the vibrating component is not affected by the centripetal force. The force analysis of the

bearing can be seen in Figure 2b.

$$\begin{cases} F_q\cos\omega t + F_1 = f_1 + G_1\cos\varphi + F_x\sin\omega t \\ F_q\sin\omega t + G_1\sin\varphi + F_x\cos\omega t = F_N + F_2 \\ F_1 = F_x\sin\omega t = m_1 r\omega^2\sin\omega t \\ f_1 = \mu_1(F_N + F_2) \\ F_2 = -ma_{x'} \\ G_1 = m_1 g \end{cases} \tag{2}$$

where, F_q is traction force of the crank, N; F_1 is inertial force of the crank terminal bearing in the y' axis, which is the direction of the bearing in contact with the slider chute, N; F_2 is inertial force of the crank terminal bearing, contact moving component, and load in the x' axis, which is the direction of movement of the slider, N; F_x is centripetal force experienced by the crank terminal bearing, N; m_1 is mass of the crank terminal bearing, kg; G_1 is gravity acting on the crank terminal bearing, N; m is total mass of the crank terminal bearing, moving component, and load, kg; f_1 is rolling friction force experienced by the crank terminal bearing while moving along the slide groove, N; f is sliding friction force experienced by the crank terminal bearing while moving along the slide groove, N; F_n is component of gravity in the direction of movement of the slider, N; μ_1 is coefficient of rolling friction between the crank terminal bearing and the slider chute; g is acceleration due to gravity, N/kg.

According to Equation (2), when an object moves perpendicular to the crank in the direction of traction at a constant speed, centripetal acceleration would be generated. From the given equilibrium equation, the force exerted by the vibrating component on the crank terminal bearing, denoted as unknown. To determine its source, a force analysis is required to be conducted for both the no-load and load-based scenarios. Additionally, the power calculation formula is as follows:

$$P_z = P\cdot(1+\delta_{\text{mei}}) = \frac{F_q v}{\eta}\cdot(1+\delta_{\text{mei}}) = \frac{T_q\omega}{\eta}\cdot(1+\delta_{\text{mei}}) \tag{3}$$

where, P is theoretical calculation of the maximum power of the motor, W; P_z is maximum power of the motor as per the actual design, W; δ_{mei} is error between experimental detection and theoretical calculation; T_q is motor drive torque, N·m; η is Motor drive efficiency.

3.1.3 Construction of no-load energy consumption model for vibrating components

Based on the contact relationship between one end of the vibrating component and the sealed shell, the static characteristics are analyzed, as shown in Figure 2c. The torque balance equation is derived.

$$\begin{cases} G_3(s_1+s_2) = G_2 b_1 + F_{\text{N1}}h_2 - F_{\text{N2}}h_1 \\ G_2 = m_2 g \\ G_3 = m_3 g \\ h_1 \approx 0,\ h_2 \approx h \\ F_{\text{N1}} = F_{\text{N2}} \end{cases} \tag{4}$$

where, G_3 is gravitational force of the connecting mechanism and fork rod, N; G_2 is gravitational force of the slider, N; s_1 is distance between the center of gravity of the connecting mechanism and outer end of the connecting mechanism, m; s_2 is distance from the outer end to y' axis when the connecting mechanism is hinged with the slider, m; b_1 is distance of the center of gravity of the slider from y' axis, m; h_1 is height of the pressure F_{N2} from the torque support point, m; h_2 is height of the pressure F_{N1} from the torque support point, m; h is height of the slider, m; F_{N1} is pressure given to the slider by the upper side housing, N; F_{N2} is pressure on the slider from the lower side housing, N; m_2 is mass of the slider, kg; m_3 is mass of the connecting mechanism and the fork rod, kg.

From Equation (4), the formulas for solving F_{N1} and F_{N2} , as well as the resistance to the motion of the vibrating component, are as follows:

$$\begin{cases} F_{\text{N1}} = F_{\text{N2}} = \dfrac{G_3(s_1+s_2) - G_2 b_1}{h} \\ F_f = \mu_2(G_2+G_3)\cos\varphi + \mu_3(F_{\text{N1}}+F_{\text{N2}}) \end{cases} \tag{5}$$

where, F_f is frictional resistance of the shell on the vibrating component for reciprocating movement along the x' axis, N; μ_2 is coefficient of friction between the lower side housing and the slider; μ_3 is coefficient of friction between the front and rear housings and the slider.

From Equations (2) and (5), combined with air resistance, it can be determined that:

$$F_{\text{N}} = F_f + kv_{x'}^2 = F_f + k\cdot(r\cdot\omega\cdot\sin\omega t)^2 \tag{6}$$

where, k is the air resistance coefficient of the vibrating components.

Based on the above analysis and the given equations, the formula for calculating the crank-driven torque can be derived as follows:

$$T_q = r\sqrt{\begin{aligned}&\left\{\mu_1\left[\mu_2(m_2+m_3)g\cos\varphi + 2\mu_3\cdot\frac{m_3 g(s_1+s_2)-m_2 g b_1}{h} + \right.\right.\\ &\left.\left. k\cdot(r\cdot\omega\cdot\sin\omega t)^2 + (m_1+m_2+m_3)r\omega^2\cos\omega t\right] + m_1 g\cos\varphi\right\}^2 + \\ &\left[\mu_2(m_2+m_3)g\cos\varphi + 2\mu_3\cdot\frac{m_3 g(s_1+s_2)-m_2 g b_1}{h} + \right.\\ &\left. k\cdot(r\cdot\omega\cdot\sin\omega t)^2 - m_1 g\sin\varphi + (m_2+m_3)r\omega^2\cos\omega t\right]^2\end{aligned}} \tag{7}$$

Combining Equation (3), we can obtain the unloaded energy consumption model as follows:

$$P = \frac{r\omega}{\eta}\sqrt{\begin{aligned}&\left\{\mu_1\left[\mu_2(m_2+m_3)g\cos\varphi + 2\mu_3\cdot\frac{m_3 g(s_1+s_2)-m_2 g b_1}{h} + \right.\right.\\ &\left.\left. k\cdot(r\cdot\omega\cdot\sin\omega t)^2 + (m_1+m_2+m_3)r\omega^2\cos\omega t\right] + m_1 g\cos\varphi\right\}^2 + \\ &\left[\mu_2(m_2+m_3)g\cos\varphi + 2\mu_3\cdot\frac{m_3 g(s_1+s_2)-m_2 g b_1}{h} + \right.\\ &\left. k\cdot(r\cdot\omega\cdot\sin\omega t)^2 - m_1 g\sin\varphi + (m_2+m_3)r\omega^2\cos\omega t\right]^2\end{aligned}} \tag{8}$$

3.1.4 Construction of energy consumption model of vibrating component with load

Assuming that the end of the fork is resisted by the branch, a set of moment equilibrium relationships are formed as shown in the specific figure below.

According to Figure 2d, the moment equilibrium equation is as follows:

$$\begin{cases} F_{\text{zu}}(s_2+s_3) = (F_{z1}+F_{z2})\times l_h/4 \\ F_{z1} = F_{z2} \end{cases} \tag{9}$$

where, F_{zu} is resistance force exerted on the fork by the branch, N; F_{z1} is pressure exerted on the slider by the right front housing, N;

F_{z2} is pressure exerted on the slider by the left rear housing, N; s_3 is distance from the contact point between the branch and the fork to the outer end of the connecting mechanism, m; l_h is length of the slider, m.

Based on the equation, we can obtain the expressions for F_{z1}, F_{z2} and the total resistance under the operating conditions of the component as follows:

$$\begin{cases} F_{z1} = F_{z2} = \dfrac{2F_{zu}(s_2+s_3)}{l_h} \\ F_z = F_{zu} + F_f + F_{zf} \\ F_{zf} = \mu_3(F_{z1}+F_{z2}) \end{cases} \tag{10}$$

where, F_{zf} is frictional force between the housing and the slider under load conditions, N; F_z is total resistance experienced by the vibrating component under loaded conditions, N.

From the above equation, we can see that F_N=F_Z, and F_{zu} represents the resistance exerted by the branch at the end. It is necessary to construct a dynamic model for the forced vibration of the fork against the branch. The specific displacement of the vibrating component with respect to the branch is assumed as follows.

From Figure 3, it can be observed that the branch is a rigid-flexible coupled composite model, with rigidity as the main component. The force analysis equation for the motion process is as follows:

$$\begin{cases} L' = \dfrac{L_2 \cdot r'}{L_1} \\ r' = r \cdot \cos\varphi \cdot \cos\omega t \\ G_4 \cdot L' = F_{zt} \cdot L_1 \\ F_{zu} = F_{zt} + F_{lz} + F_{kz} \\ F_{lz} = k_2 m_4 r\omega^2 \cdot \cos\varphi \cdot \cos\omega t \\ F_{kz} = k_1 \cdot (r \cdot \omega \cdot \sin(\omega t + \beta))^2 \end{cases} \tag{11}$$

where, L' is displacement of the center of mass of the branch when acted upon by the fork, m; L_2 is distance between the center of mass of the branch and the constrained end of the swinging branch, m; L_1 is distance between the point of action of the fork on the branch and the constrained end of the swinging branch, m; G_4 is total load weight, N; F_{zt} is resistance exerted by the branch on the fork, N; F_{kz} is air resistance experienced by the vibrating component and the branch, N; k_1 is comprehensive air resistance coefficient that considers the high-speed movement of the branch and the vibrating component' operation; k_2 is correction coefficient for the overall inertia force experienced by the forced vibrating branch; β is phase lag of the swinging branch's reciprocating speed, rad; F_{lz} is inertia force experienced by the forced motion of the branch, N.

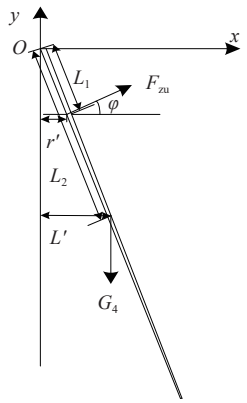

Figure 3 Force diagram of Chinese wolfberry branches under the action of fork bar

In conclusion, the resistance and torque experienced by the crankshaft's end bearing are as follows:

$$\begin{aligned} F_N = &\left(\frac{m_4 g L_2 r}{L_1^2} + k_2 m_4 r\omega^2\right) \cdot \frac{l_h + 4\mu_3(s_2+s_3)}{l_h} \cdot \cos\varphi \cdot \cos\omega t + \\ &\mu_2(m_2+m_3)g\cos\varphi + 2\mu_3 \cdot \frac{m_3 g(s_1+s_2) - m_2 g b_1}{h} + \\ &k_1 \cdot (r \cdot \omega \cdot \sin(\omega t + \beta))^2 \end{aligned} \tag{12}$$

$$\begin{aligned} T_q = r \sqrt{} &\left\{\mu_1\left[\left(\frac{m_4 g L_2 r}{L_1^2} + k_2 m_4 r\omega^2\right) \cdot \frac{l_h + 4\mu_3(s_2+s_3)}{l_h} \cdot \cos\varphi \cdot \cos\omega t + \mu_2(m_2+m_3)g\cos\varphi + m_1 g\cos\varphi + \right.\right. \\ &\left.\left. 2\mu_3 \cdot \frac{m_3 g(s_1+s_2) - m_2 g b_1}{h} + k_1 \cdot (r \cdot \omega \cdot \sin(\omega t + \beta))^2 + (m_1+m_2+m_3) r\omega^2 \cos\omega t\right]\right\}^2 + \\ &\left[\left(\frac{m_4 g L_2 r}{L_1^2} + k_2 m_4 r\omega^2\right) \cdot \frac{l_h + 4\mu_3(s_2+s_3)}{l_h} \cdot \cos\varphi \cdot \cos\omega t + \mu_2(m_2+m_3)g\cos\varphi + \right. \\ &\left. 2\mu_3 \cdot \frac{m_3 g(s_1+s_2) - m_2 g b_1}{h} + k_1 \cdot (r \cdot \omega \cdot \sin(\omega t + \beta))^2 - m_1 g\sin\varphi + (m_2+m_3) r\omega^2 \cos\omega t\right]^2 \end{aligned} \tag{13}$$

Combining with Equation (3), the load energy consumption model can be derived as follows:

$$\begin{aligned} P = \frac{r\omega}{\eta} \sqrt{} &\left\{\mu_1\left[\left(\frac{m_4 g L_2 r}{L_1^2} + k_2 m_4 r\omega^2\right) \cdot \frac{l_h + 4\mu_3(s_2+s_3)}{l_h} \cdot \cos\varphi \cdot \cos\omega t + \mu_2(m_2+m_3)g\cos\varphi + m_1 g\cos\varphi + \right.\right. \\ &\left.\left. 2\mu_3 \cdot \frac{m_3 g(s_1+s_2) - m_2 g b_1}{h} + k_1 \cdot (r \cdot \omega \cdot \sin(\omega t + \beta))^2 + (m_1+m_2+m_3) r\omega^2 \cos\omega t\right]\right\}^2 + \\ &\left[\left(\frac{m_4 g L_2 r}{L_1^2} + k_2 m_4 r\omega^2\right) \cdot \frac{l_h + 4\mu_3(s_2+s_3)}{l_h} \cdot \cos\varphi \cdot \cos\omega t + \mu_2(m_2+m_3)g\cos\varphi + \right. \\ &\left. 2\mu_3 \cdot \frac{m_3 g(s_1+s_2) - m_2 g b_1}{h} + k_1 \cdot (r \cdot \omega \cdot \sin(\omega t + \beta))^2 - m_1 g\sin\varphi + (m_2+m_3) r\omega^2 \cos\omega t\right]^2 \end{aligned} \tag{14}$$

3.2 Energy consumption model simulation and analysis of reciprocating vibration for Chinese wolfberry picking

Building on the previous research foundation, a multi-parameter adjustable reciprocating vibration test bed and optimal operating parameters for Chinese wolfberry harvesting device, the input parameter values for the energy consumption model under the conditions of optimal operating parameter configuration are determined through measurements of the installation dimensions of the vibrating component, and the friction coefficient between steel materials with certain roughness together with parameterization of

the branch model in the preliminary stage are referenced. The following are the input parameter values under the optimal operating parameter configuration: s_1=0.1 m, s_2=0.02 m, s_3=0.13 m, μ_1=0.02–0.08, μ_2=0.1–0.15, μ_3=0.1–0.15, m_1=0.008 kg, m_2=0.079 kg, m_3=0.064 kg, m_4=0.02 kg (set the quality of one Chinese wolfberry branch), r=0.015 m, l_h=0.05 m, h=0.056 m, b_1=0.005 m, η=0.9, L_1=0.183 m, L_2=0.217 m, g=9.8 N/kg, ω=125.6 rad/s. In this study, simulation and experimental verification are carried out from the aspect that the vibrating components are perpendicular to the vertical line, and set $\varphi = 0$.

3.2.1 Simulation and analysis of no-load energy consumption model

According to Equation (7), combined with the parameters mentioned above, data calculations and plotting are carried out with Matlab7.1 to obtain the trend chart of the driving torque of the vibrating component, and the power trend can be obtained combined with Equation (8). In the following section, the influence of different vibration frequencies on energy consumption is analyzed firstly. Next, based on the optimal operating vibration frequency[23] of 20 Hz, the simulations are performed to analyze the other parameters that affect energy consumption. The details are shown below:

(1) Analysis of the influence of vibration frequency on torque

Based on the torque model given by Equation (7), different frequencies of 2.5 Hz, 5 Hz, 10 Hz, and 20 Hz are selected. The torque variation curves are simulated and obtained. Please refer to Figure 4 for more details.

From Figure 4a, it can be observed that the torque curves 1, 2, 3, and 4 correspond to frequencies from low to high. As the vibration frequency increases, the torque increases significantly. Torque curve 4 corresponds to an input frequency of 20 Hz. Under this high-frequency operating condition, the following section will investigate the influence of other parameters on the torque.

(2) Analysis of the influence of friction coefficient on torque

Considering data 1: μ_1=0.02, μ_2=0.1, μ_3=0.1. data 2: μ_1=0.08, μ_2=0.1, μ_3=0.1. Data 3: μ_1=0.02, μ_2=0.15, μ_3=0.15. Neglecting air resistance, the effects of rolling friction of the bearing and sliding friction between the cover plate and the vibrating component on the torque are explored. From Figure 4b, it can be observed that torque curves 1, 2, and 3 are corresponded with the three sets of dynamic and static friction parameter configurations mentioned above. From the curve graph, it can be concluded that the dynamic and static friction coefficients have a negligible effect on the torque (power) within their respective ranges. When the period is 0 and T, the driving torque is slightly higher than the torque at $T/2$ due to the effect of gravity on the crankshaft end bearing according to the energy consumption model. Additionally, at angles $T/4$ and $3T/4$, the driving torque is close to 0, indicating that the maximum speed of reciprocating motion occurs along the x' axis and the acceleration is zero. At this point, the driving torque only overcomes the sliding friction force of the vibrating component, and the torque caused by the friction resistance can be neglected.

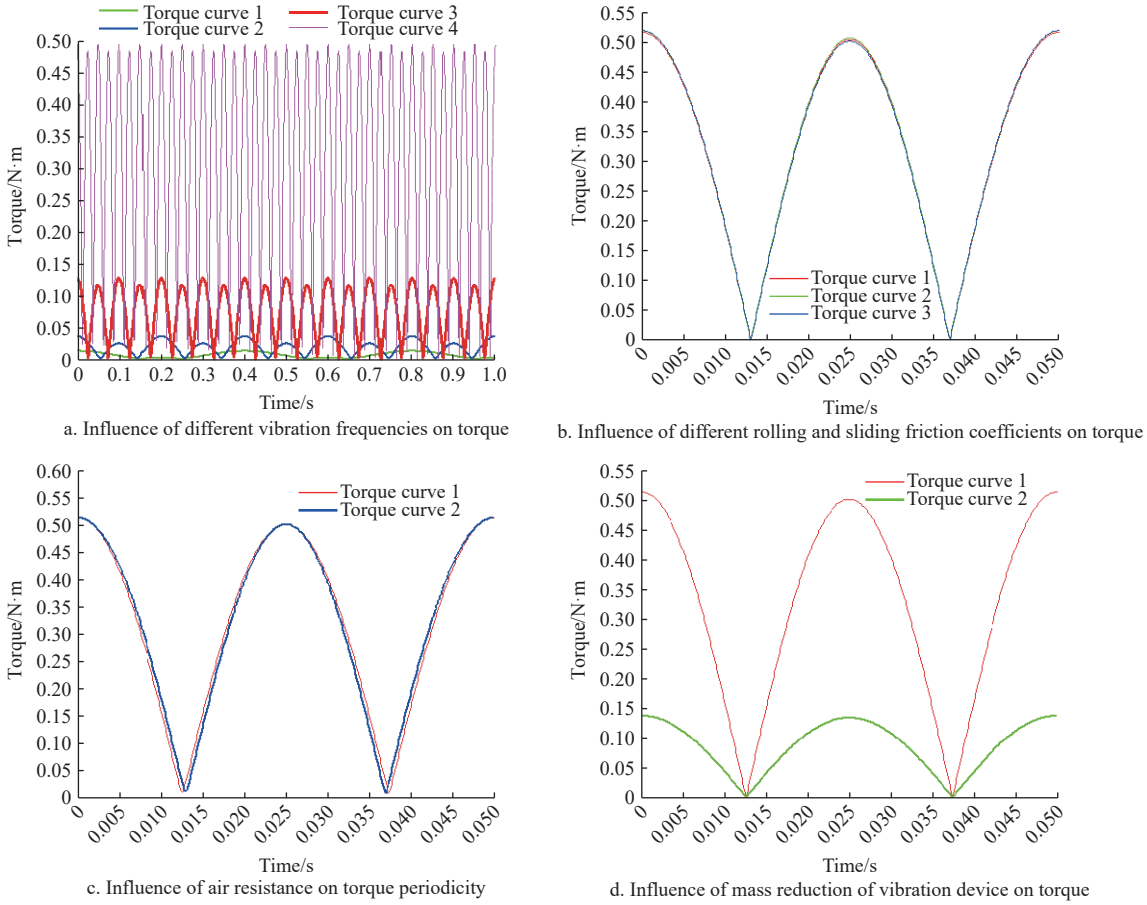

Figure 4 Influence of parameters on torque under no-load condition

(3) Analysis of the influence of air resistance coefficient on torque

To study the effect of air resistance on the reciprocating motion of the vibrating component, the air resistance coefficient k is taken as 0 and 0.25, with m_2 = 0.079 kg and m_3 = 0.064 kg, and the simulation results are compared as follows.

From Figure 4c, it can be observed that when air resistance is added, the thick blue curve, compared to the thin red curve, is able

to shorten the period between adjacent minimum torques, and the minimum torque would slightly increases. However, the influence on the overall torque of the system can be neglected.

(4) Analysis of the influence of vibrating component mass on torque

Based on two types of Chinese wolfberry reciprocating vibration picking devices, the mass of the vibrating component is measured, and the results are as follows: m_2 = 0.079 kg, m_3 = 0.064 kg and m_2 = 0.023 kg, m_3 = 0.015 kg. Without other parameters changed and air resistance considered, the influence of vibrating component mass on torque is studied, as shown in Figure 4d, from which can be observed that the larger mass of the vibrating component has, the greater driving torque and the higher power consumption will be generated. When the vibrating component is designed, it is preferred to have a smaller mass while ensuring a certain strength and stiffness, based on the requirements of load force vibration. For a small group of vibrating component, the maximum torque is 0.14 N·m, and according to Equation (8), the required power is 19.5 W. It is verified that the design power of the hand-held Chinese wolfberry vibration picking device which selecting power 30W is reasonable[23].

In addition, for the data with a larger vibrating component mass, the corresponding maximum torque is 0.52 N·m, and according to Equation (8), the required power is 72.49 W. On the other hand, without the friction and air resistance considered, the maximum torque for the reciprocating vibration of the vibrating component is 0.50 N·m, and the required power is 69.68 W. Therefore, under high-frequency (20 Hz) and low-amplitude (15 mm) vibration conditions, both the vibrating component and the load mass play a dominant role in energy consumption.

3.2.2 Simulation analysis of load energy consumption model

(1) Analysis of the impact of load air resistance phase on torque

According to Equation (12), with the design conditions of m_2 = 0.079 kg and m_3 = 0.064 kg for the vibrating component, a simulation analysis with added load is conducted. One load with a mass of m_4 = 0.02 kg is selected. Considering the air resistance conditions and the significant influence of branches and components on the air, the resistance coefficient is increased compared to the unloaded operation, with k_1 = 0.5 enhanced. At the same time, considering the vibration of branches with leaves and the lag in energy transfer, the air resistance phase β is taken as 0, 0.785, and 1.57 to study their impact on the system torque. The load inertia coefficient k_2 is taken as 1. Please refer to Figure 5 for details.

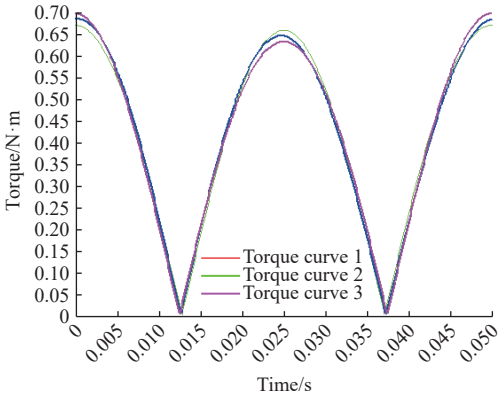

Figure 5 Influence of air resistance phase on torque of vibrating device with load

From Figure 5, it can be observed that the torque corresponding to 0 and T cycles significantly increases with the phase increasing, while the torque corresponding to T/2 cycle slightly decreases instead. The air resistance phase has a significant impact on the magnitude of torque.

(2) Analysis of torque effects for different loads

Based on Equation (12) and the design conditions of the vibrating component, a simulation analysis with added load is conducted. Following the typical model of summer fruit, the starting position of the vibration of the third branch is simulated. Each branch has a mass of 0.02 kg, and four groups of loads with increasing branch mass in arithmetic progression, including 1 branch, 3 branches, 5 branches, 7 branches, and 9 branches, which are selected for simulation. The air resistance coefficient is set to 0.5. Additionally, a velocity phase difference of 0.785 is chosen, and the load inertia coefficient is set to 1. The torque effects can be seen in detail in Figure 6a.

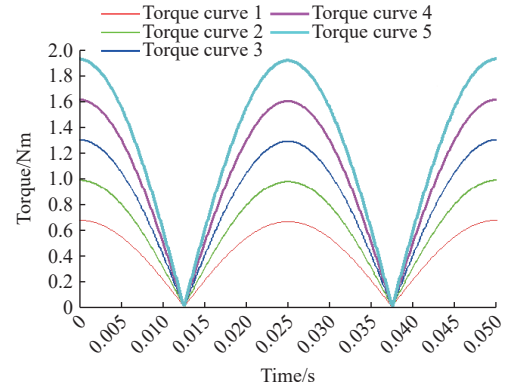

a. Influence of different load on torque when setting k_2 as 1

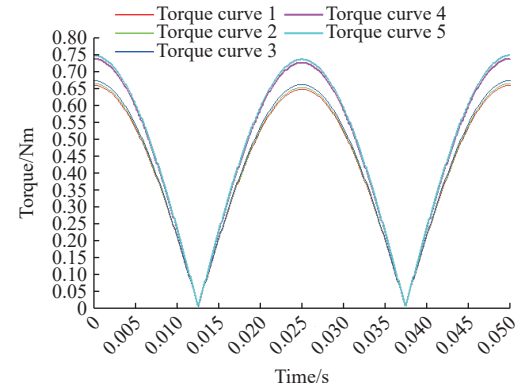

b. Influence of different load on torque when k_2 is corrected

Figure 6 Torque simulation of inertia force correction coefficient under different load conditions

From Figure 6a, it can be observed that as the load increases, the driving torque of the vibrating device increases. The maximum torques consumed by the five groups of loaded branches are 0.68 N·m, 1.00 N·m, 1.31 N·m, 1.62 N·m, and 1.94 N·m, respectively. Based on the torque variations, the maximum torque is obtained, and considering Equation (3), the corresponding maximum power outputs are determined to be 94.77 W, 139.37 W, 182.57 W, 225.78 W, and 270.37 W. In the following section, these simulation results will be validated and adjusted through experiments.

4 Experiments of the energy consumption for vibrating device

4.1 Energy consumption detection system

4.1.1 Torque electric signal detection system base on AC servo motor

In order to investigate the energy consumption mechanism of the reciprocating vibration-type Chinese wolfberry picking device, a

real-time monitoring system for speed and driving torque combined with the previous simulation analysis based on the energy consumption model, driven by an AC servo motor, is developed. The key components of the selected motor are from YELCHM (model 60Sm013030), with a rated power of 400 W, a rated torque of 1.3 N·m (instantaneous maximum torque of 5.73 N·m), a rated speed of 3000 r/min, and a driving voltage of 220 V. A high-frequency, low-amplitude vibration acquisition test bench is designed, with an adjustable frequency range of 0-50 Hz and a set amplitude of 15 mm. Furthermore, a TPC7022Ei touchscreen controller is chosen, with a minimum data acquisition time of 10ms. The real-time torque and speed acquisition interface is built on the touchscreen controller. The touchscreen controller interface on the upper computer is compatible with the AC servo motor on the lower computer. Serial communication is established through the RS485 bus, using the compatible MODBUS-RTU protocol as the underlying communication protocol[24]. Torque and speed data are directly read from the servo drive which providing the necessary tools for the verification experiment. The data acquisition during the experiment is shown in Figure 7.

Figure 7 Testing ground of torque data acquisition system of vibration test bench

4.1.2 Torque sensing detection system

According to the internal electrical signal of AC servo, the detection is unstable, and the minimum acquisition interval cannot meet the requirements of verifying the torque change trend, and it is not conducive to searching for the maximum torque value. Therefore, in this study, a high-precision torque sensor, a matching filter amplifier and an industrial data acquisition system are added between the output shaft of the AC servo motor and the vibration parts, as shown in Figure 8.

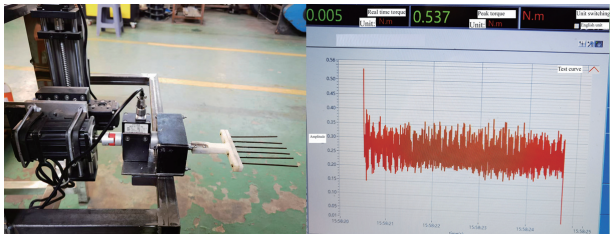

Figure 8 Torque sensing detection system

As can be seen from Figure 8, the AC servo motor is connected with the torque sensor through the coupling, and the output shaft at the other end of the sensor provides the driving force for the vibration component. By detecting the torque change of the output shaft of the AC servo motor, it provides an important means for actual torque detection and theory verification. The sensor connects the data signal with the filter amplifier through RS485 bus (MODBUS-RTU protocol) and processes it. Finally, it interacts with the industrial signal measurement system installed in the upper computer through RS485 conversion interface.

CL1-202-2N·m torque sensor is adopted, with a measuring range of 2 N·m, an output signal of 1.294 mV/V, an accuracy of 0.2%FS, and a power supply of 5-12 VDC.

4.2 Experiments

According to YELCHM control system, the operation cycle is set to 50ms (frequency is 20 Hz) for driving operation. Through the torque sensing detection system, data can be read once every 2 ms, and 25 groups of data can be read in one cycle. The specific tests are as follows.

4.2.1 Verification of no-load torque curve and analysis of torque error

Through the torque sensing detection system, the data of torque under no-load operation conditions are collected. In this study, 25 groups of data are extracted in one cycle, and the change trend is shown in Figure 9. In addition, in order to search for the maximum torque of the system and expand the data collection, the maximum torque is selected as a reference, and 1000 sets of 2 s data are selected from the torque data storage table, from which 20 sets of maximum torque data are selected, as shown in Table 1.

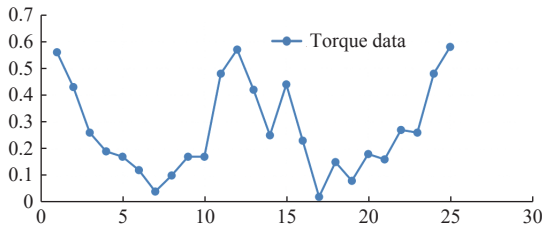

Figure 9 No-load detection torque trend chart

Table 1 Extraction of actual maximum torque in no-load condition

Index	1	2	3	4	5	6	7	8	9	10
T_{qmax}/N·m	0.57	0.56	0.56	0.54	0.54	0.52	0.53	0.53	0.52	0.52
Index	11	12	13	14	15	16	17	18	19	20
T_{qmax}/N·m	0.52	0.51	0.54	0.57	0.57	0.51	0.54	0.54	0.52	0.52

As can be seen from Figure 9, the trend of torque data is consistent with Figure 4, and the data fluctuates due to system vibration. The torque model is verified to be accurate.

According to the table above, the maximum torque is 0.57 N·m, corresponding to a power of 79.46 W. The simulated maximum torque in the no-load condition is 0.52 N·m, requiring a power of 72.50 W. The experimental detection and theoretical calculation error δ_{mei} is 0.096, which is equivalent to 9.6%. The actual torque is slightly higher than the theoretical value, which can be attributed to system structure and installation errors. This verifies the reasonableness of the theoretical model for energy consumption in the reciprocating vibration-type Chinese wolfberry picking device

under no-load conditions.

4.2.2 Load coefficient adjustment and verification based on torque error

Based on the conditions and conclusions of the no-load experiment, four sets of branches with masses of 20 g, 60 g, 100 g, 140 g, and 180 g are prepared. Due to the limitation of the testing cycle, in order to observe the influence of the load on torque and ensure that the quality of the vibrating process remains constant for each set of branches, branches of equal mass are selected for the experiment. The data for each set of branches is extracted using the same method as the no-load condition, and the data is organized as shown in the following table.

According to Table 2, under the condition of high-frequency low-amplitude vibration, the excitation force applied to the Chinese wolfberry branches by the vibrating components, the change in branch mass has no significant influence on the torque. The maximum torque values corresponding to the five groups of branch loads are 0.73 N·m, 0.74 N·m, 0.75 N·m, 0.82 N·m, and 0.83 N·m. The simulation results do not match those shown in Figure 6a, indicating that as the load increases, the variation in the excitation force applied to the branches by the vibrating components is small. Therefore, the overall amplitude of the load inertial force needs to be adjusted. Using the unloaded vibration torque error as 0.096, with the detection results as a reference, and the system error deducted, the theoretical simulation values are obtained as 0.670 N·m, 0.675 N·m, 0.684 N·m, 0.748 N·m, and 0.757 N·m, respectively. Then, comparing with the simulated maximum torque in Figure 6a, the correction factors are calculated as 0.910, 0.312, 0.197, 0.198, and 0.160, respectively. The overall amplitude parameters of the forced vibration of the loaded branches are determined as 13.65 mm, 4.68 mm, 2.96 mm, 2.97 mm, and 2.40 mm. The actual torque curves after correction are shown in Figure 6b. The correction relationship for the five groups of loaded branches is summarized in Table 3.

Table 2 Extraction of actual maximum torque under different loads

No.	1	2	3	4	5	6	7	8	9	10	11	12	13	14	15	16	17	18	19	20
T_{q1max}/N·m	0.56	0.73	0.66	0.66	0.56	0.68	0.68	0.70	0.70	0.70	0.66	0.66	0.66	0.66	0.66	0.69	0.69	0.69	0.68	0.68
T_{q2max}/N·m	0.72	0.72	0.72	0.66	0.66	0.66	0.70	0.70	0.70	0.68	0.68	0.64	0.64	0.65	0.65	0.73	0.73	0.73	0.74	0.74
T_{q3max}/N·m	0.74	0.74	0.74	0.65	0.65	0.74	0.75	0.60	0.73	0.73	0.68	0.68	0.73	0.72	0.72	0.73	0.73	0.68	0.68	0.74
T_{q4max}/N·m	0.78	0.78	0.82	0.82	0.82	0.73	0.73	0.75	0.75	0.69	0.69	0.69	0.66	0.66	0.69	0.69	0.73	0.74	0.75	0.78
T_{q5max}/N·m	0.77	0.77	0.73	0.74	0.69	0.73	0.78	0.78	0.82	0.82	0.79	0.79	0.83	0.69	0.68	0.74	0.75	0.75	0.78	0.77

Table 3 Relationship between load mass and related parameters

Index	1	2	3	4	5
m_4/kg	0.02	0.06	0.10	0.14	0.18
$T_{qi\max}$/N·m	0.73	0.74	0.75	0.82	0.83
ΔT_q	0.16	0.17	0.18	0.25	0.26
k_2	0.910	0.312	0.197	0.198	0.160
Load amplitude/mm	13.65	4.68	2.96	2.97	2.40

In addition, fitting the load branch mass to the actual torque shows that polynomial functions up to the 5th degree satisfy the requirements. However, for simplicity of calculation, a 2nd degree polynomial is chosen as the fitting result, given by P=2.6786m^2+0.164 29m+0.722 21, with an error of 0.028 685. This fitting polynomial can be used to predict the actual power consumption for load masses between 20 g and 180 g. Taking a 40 g branch load as an example, with a measured torque value of 0.74, the calculated result using the fitting equation is 0.733 N·m, corresponding to a power of 102.2 W. The deviation from the fitting error is 0.95%. Following this calculation procedure, it is possible to guide the selection of drive motors for different load limits.

5 Conclusions

This study aims to construct an energy consumption model, perform simulations, and conduct experimental verification to analyze the structure and motion of the reciprocating vibration Chinese wolfberry harvesting device. The following conclusions are drawn:

(1) The characteristics of crankshaft bearing, empty and loaded motion of the vibrating components, and force analysis are analyzed. A theoretical energy consumption model for the reciprocating harvesting device is established. The following results are obtained by the simulation analysis of the model: The torque is influenced significantly by the friction coefficient, the vibrating components and load mass. The cycle between adjacent minimum torques is shorten by the air resistance coefficient, but the effect of which on the overall torque of the system can be neglected. The phase of air resistance has a more significant impact on the torque magnitude. The theoretical calculation of the maximum power of the motor and the relationship between the vibrating components and load mass are obtained, providing a theoretical basis for experimental verification.

(2) An AC servo motor torque detection system and a torque sensing detection system are constructed separately, and then experiments are carried out, the following results are obtained: Under the condition of no load and a motor speed frequency of 20 Hz, the torque model is verified to be accurate. The maximum torque measured is 0.57 N·m, corresponding to a power of 79.46 W. When compared with the maximum torque of 0.52 N·m obtained from the no-load simulation, the error is within 9.6%. Under the loaded condition, the maximum torque values measured for the five groups of branch loads are 0.73 N·m, 0.74 N·m, 0.75 N·m, 0.82 N·m, and 0.83 N·m, respectively. The small impact of load branch mass on the torque indicates a weak correlation between the output excitation force and the load branch mass. Based on these findings, a model is fitted to establish the relationship between the load and torque, providing guidance for motor selection.

To sum up, under the condition of achieving ideal fruit removal effect, the motor power for the vibration unit of the large Chinese wolfberry harvester is at least 103 W and torque is 0.83 N·m. However, the motor no-load power for the hand-held Chinese wolfberry vibration picker is 19.5 W and torque is 0.14 N·m, and the actual load is a single branch, there is little difference between the newly added torque and power, which fully shows that it is necessary to reduce the mass of vibration component.

(3) This study has revealed the load limits and motor selection criteria for the reciprocating vibration Chinese wolfberry harvesting device under certain excitation force conditions (amplitude of 15 mm, frequency of 20 Hz), with the reciprocating vibration being

parallel to the horizontal direction. It provides guidance for motor selection in the reciprocating vibration Chinese wolfberry harvesting device under different load limit conditions. At the same time, the exciting force given by the vibrating component to branches with different loads is determined. This provides an important basis for understanding the mechanism of fruit detachment in Chinese wolfberry branches under forced reciprocating vibration. Ultimately, it lays the foundation for achieving high-quality operations in Chinese wolfberry harvesting machines based on an array of reciprocating vibration units.

(4) Based on the requirements of large-scale harvesting device for complex operating environments with multiple branches, this study focuses on designing vibrating components with larger mass (m_2 = 0.079 kg, m_3 = 0.064 kg). In the later stages, the research objectives shift towards lightweight design and energy efficiency evaluation. By employing new materials and structural optimization as means, and the same research approach can be applied again to obtain the motor selection decisions by employing new materials and structural optimization as means, and load limits for the optimized vibrating components.

Acknowledgements

This work is supported by National Natural Science Foundation of China (Grant No. 32201681), the Ningxia Hui Autonomous Region Science and Technology Program (Grant No. 2021BEF02001) and The Fruit, Vegetable and Tea Harvesting Machinery Innovation Project of the Chinese Academy of Agricultural Sciences.

[References]

[1] Ma J W. Research status and prospect of the mechanized technology of picking wolfberry in China. Mechanical Research & Application, 2017; 30(4): 151–153. (in Chinese)

[2] Cao L, Zhang A L. Study on present situation development stages and trends of Chinese wolfberry industry. Forest Resources Management, 2015(2): 4–8, 30. (in Chinese)

[3] Wang Y J, An W, Shi Z G, Zhao J H. Research progress in wolfberry medicinal properties. Journal of Anhui Agricultural Science, 2020; 36(30): 13213–13214, 13218. (in Chinese)

[4] Luo X W. Artificial intelligence and plant protection mechanization. Journal of Intelligent Agricultural Mechanization, 2020; 1(1): 1–6. (in Chinese)

[5] Sun Y T, Chen G, Li Q L, Sun Y J, Shen J X, Yan N. Application and development trend of intelligent agriculture. Journal of Intelligent Agricultural Mechanization, 2020; 1(1): 56–59. (in Chinese)

[6] Song Z Y, Mei S, Xiao H R, Shi Z G, Wang J P, Zhao Y, Ding W Q. Comparative test and analysis on the harvesting methods of Chinese wolfberry fruit. Journal of Chinese Agricultural Mechanization, 2019; 40(10): 110–116. (in Chinese)

[7] Li C, Xing J J, Xu L M, He S L, Li S J. Design and experiment of wine grape threshing mechanism with flexible combing striping monomer. Transactions of the CSAE, 2015; 31(6): 290–296. (in Chinese)

[8] Ye L Q, Li Q, Chen J Y, An W. Study on picking performance of portable wolfberry picker. Ningxia Journal of Agriculture and Forestry Science and Technology, 2009; 4: 4–5, 56. (in Chinese)

[9] Zhang W Q, Zhang M M, Zhang J X, Li W. Design and experiment of vibrating wolfberry harvester. Transactions of the CSAM, 2018; 49(7): 97–102. (in Chinese)

[10] Cao Y L. Chinese wolfberry picker: China Patent, ZL201020520858.8. 2011.08. 31. (in Chinese)

[11] Zhao Y W, Huang H R, Liu X M, Zhang W Y, Geng D X. Design and Grasping Experiments. Transactions of the CSAM, 2023; 54(9): 74–84. (in Chinese)

[12] Qin Z Y, Gao S, Shi T F, Chen Y. One kind of vibrating Chinese wolfberry picking machine: China patent, ZL201922364289.6. 2020.10. 13. (in Chinese)

[13] Shi B G, Yang W Z. Development status and countermeasures of organic wolfberry industry in Qinghai Province. Journal of Anhui Agricultural Science, 2019; 47(7): 229–231. (in Chinese)

[14] He M, Li C S, Wang L H, Zhang Y O, Yang L T, Wu S. Research status of the harvesting device of *Lycium barbarum* L. Journal of Anhui Agricultural Science, 2015; 43(33): 367 - 369, 385. (in Chinese)

[15] Zhang Z, Xiao H R, Ding W Q, Mei S. Mechanism simulation analysis and prototype experiment of Chinese wolfberry harvest by vibration mode. Transaction of the CSAE, 2015; 31(10): 20–28. (in Chinese)

[16] Liu W H. Development and experimental effect of self-propelled large *Lycium barbarum* picker. Agriculture Machinery Technology Extension, 2014; 1: 47–48. (in Chinese)

[17] Peng Y, Zhang Z Y, Liu Y, Xu T S, Wang R J. Design and experiment of accurate clamping vibration wolfberry harvesting machine. Mechanical Research & Application, 2018; 31(6): 123–129, 132. (in Chinese)

[18] Silva F C D, Silva F M D, Alves MC, Ferraz G A E S, Sales RS. Efficiency of coffee mechanical and selective harvesting in different vibration during harvest time. Coffee Science, 2015; 10(1): 56–64.

[19] Du X Q, Li D W, He L Y, Wu C Y, Lin L P. Fruit motion analysis in process of mechanical vibration harvesting based on electronic fruit technique. Transactions of the CSAE, 2017; 33(17): 58–64. (in Chinese)

[20] Liu J Z, Tang S Q, Shan S, Ju J, Zhu X X. Simulation and test of grape fruit cluster vibration for robotic harvesting. Transactions of the CSAM, 2016; 47(5): 1–7. (in Chinese)

[21] Challa V R, Prasad M G, Shi Y, Fisher F T. A vibration energy harvesting device with bidirectional resonance frequency tunability. Smart Materials & Structures, 2008; 17(1): 15035–15010.

[22] Mei S, Xiao H R, Shi Z G, Jiang Q H, Zhao Y, Ding W Q. Design and test of low-loss Chinese wolfberry harvesting technology and equipment based on reciprocating vibration method. Journal of Chinese Agricultural Mechanization, 2019; 40(11): 100–105, 208. (in Chinese)

[23] Mei S, Wang J P, Song Z Y, Tang D B, Shen C. Mechanism and experimental study on the fruit detachment of Chinese wolfberry through reciprocating vibration. Int J Agric & Biol Eng, 2024; 17(2): 47–58.

[24] Mei S, Pei F Q, Song Z Y, Tong Y F. Design and testing of accurate dicing control system for fruits and vegetables. Actuators, 2022; 11(9): 1–19.